Depicting pseudotime-lagged causality across single-cell trajectories for accurate gene-regulatory inference

Caleb C. Reagor[1,2*], Nicolas Velez-Angel[1], and A. J. Hudspeth[1*]

[1] Howard Hughes Medical Institute and Laboratory of Sensory Neuroscience, The Rockefeller University, New York, NY, USA

[2] Tri-Institutional PhD Program in Computational Biology and Medicine, New York, NY, USA

[*] E-mail contacts creagor@rockefeller.edu and hudspaj@rockefeller.edu

Abstract

Identifying the causal interactions in gene-regulatory networks requires an accurate understanding of the time-lagged relationships between transcription factors and their target genes. Here we describe DELAY, a convolutional neural network for the inference of gene-regulatory relationships across pseudotime-ordered single-cell trajectories. We show that combining supervised deep learning with joint-probability matrices of pseudotime-lagged trajectories allows the network to overcome important limitations of ordinary Granger causality-based methods, such as the inability to infer cyclic relationships such as feedback loops. Our network outperforms several common methods for inferring gene regulation and predicts novel regulatory networks from scRNA-seq and scATAC-seq datasets given partial ground-truth labels. To validate this approach, we used DELAY to identify important genes and modules in the regulatory network of auditory hair cells, as well as likely DNA-binding partners for two hair cell cofactors (Hist1h1c and Ccnd1) and a novel binding sequence for the hair cell-specific transcription factor Fiz1. We provide an open-source implementation of DELAY at https://github.com/calebclayreagor/DELAY.

Introduction

Single-cell sequencing technologies can provide detailed data for the investigation of heterogeneous populations of cells collected at specific times—so-called "snapshots"—during cellular differentiation or dynamic responses to stimulation[1]. However, owing to inherent delays in molecular processes such as transcription and translation, static measurements from individual cells cannot reveal the causal interactions governing cells' dynamic responses to developmental and environmental cues[2,3,4]. Because population-level heterogeneity in tissues often reflects the asynchronous progression of single cells through time-dependent processes, observed patterns of gene expression can nonetheless indicate the stages of development to which individual cells belong[5]. Many algorithms exploit these cell-to-cell differences to infer dynamic trajectories and reconstruct cells' approximate temporal progressions along inferred lineages in pseudotime[6,7].

Several methods for gene-regulatory inference rely on pseudotime in Granger causality tests, which try to determine whether new time series can add predictive power to inferred models of gene regulation[8,9]. However, Granger causality-based methods can be error-prone when genes display nonlinear or cyclic interactions, or when the sampling rate is uneven or too low[9,10,11,12]. Because pseudotime trajectories exhibit these problems, Granger causality-based methods often underperform model-free approaches that exploit pure statistical dependencies in gene-expression data[9,13,14].

By contrast, deep learning-based methods make no assumptions about the temporal relationships or connectivity between genes in complex regulatory networks; instead, these data-driven approaches learn general features of regulatory interactions[15,16]. Here we describe a deep learning-based method termed DELAY (*De*picting *La*gged Causalit*y*) that learns gene-regulatory interactions from discrete joint-probability matrices of paired, pseudotime-lagged gene-expression trajectories. Our data suggest that DELAY can address many shortcomings of current Granger causality-based methods and provide a useful, complementary approach to overcome common limitations in the inference of gene-regulatory networks from single-cell data.

50 # Results

51 **A convolutional neural network predicts pseudotime-lagged gene-regulatory relationships.**

52 To predict gene-regulatory relationships from single-cell data, we developed a convolutional
53 neural network based on Granger causality[17]. The input to DELAY consisted of stacks of two-
54 dimensional joint-probability matrices for pairs of transcription factors, putative target genes, and
55 highly correlated "neighbor" genes[18]. We constructed the input matrices by aligning the gene-
56 expression trajectories of a transcription factor *A* at several lagged positions in pseudotime relative
57 to a target gene *B* to generate joint-probability distributions from two-dimensional histograms of
58 gene coexpression at each lag (Fig. 1a). Each input matrix consisted of the L2-normalized cell-
59 number counts from a two-dimensional gene-coexpression histogram with 32 fixed-width bins in
60 each dimension, spanning each gene's minimum and maximum expression values. Although the
61 marginal probability distributions for both *A* and *B* remained essentially unchanged at each lag
62 except for cells lost at the leading and lagging edges of the shifted trajectories, realigning the gene
63 expression in pseudotime altered key features of the resulting joint-probability matrices. In other
64 words, causally related genes share important pseudotime-lagged patterns of gene coexpression
65 with nearby cells in single-cell trajectories.

66 Using ground-truth labels from cell type-specific chromatin-immunoprecipitation
67 sequencing (ChIP-seq)[14], we conducted supervised learning to train our neural network to predict
68 whether *A* directly regulates *B*. This procedure resembled a regression in a Granger causality test[17],
69 in which values of a time series Y at timepoints y_t are regressed against values from another time
70 series X at timepoints $x_t, x_{t-1}, x_{t-2}, \ldots, x_{t-T}$ up to some maximum lag T to determine whether any
71 time-lagged values of X add explanatory power to Y's autoregressive model. DELAY likewise
72 learned higher weights for gene-coexpression matrices at specific pseudotime lags that indicated
73 the true regulatory relationship between genes. After comparing several neural network
74 architectures, we selected a six-layered convolutional network trained on pseudotime-aligned
75 (T=0) and five pseudotime-lagged ($T \in \{1,2,3,4,5\}$) gene-coexpression matrices to predict direct

76 gene-regulatory relationships (Fig. 1b, Supplementary Fig. 1). We also trained the network on
77 lagged-coexpression matrices of two highly correlated neighbor genes per gene, that is, the two
78 transcription factors with the highest cross-correlation with *A* and *B* along the single-cell
79 trajectory. Because the neighbor genes can present stronger alternatives to the primary hypothesis
80 that *A* directly regulates *B*, including these matrices for *A* and *B* *versus* their highly-correlated
81 transcription factors reduced false-positive predictions.

82 **DELAY outperforms several common methods of gene-regulatory inference.**

83 We trained DELAY on gene-expression datasets from human embryonic stem cells (hESCs)[19],
84 mouse embryonic stem cells (mESCs)[20], and three lineages of mouse hematopoietic stem cells
85 (mHSCs)[21]. We generated separate training datasets for each of the hematopoietic lineages, and
86 all datasets contained at least four hundred cells per lineage (Table 1). Each trajectory was oriented
87 according to known experimental timepoints or precursor-cell types and lineages, and pseudotime
88 values were inferred separately with Slingshot[6] for each lineage (Supplementary Fig. 2). We chose
89 these datasets because the cell types and trajectories are well characterized and offer cell type-
90 specific ChIP-seq data to generate ground-truth networks[14]. Although the three hematopoietic
91 datasets contained similar numbers of examples of true regulation and no interaction, both of the
92 embryonic datasets were class-imbalanced and contained fewer examples of true regulation. To
93 avoid overfitting, we performed five-fold cross validation on randomly segregated 70 %-30 %
94 splits of all possible gene-pair examples, that is, both true regulation and no interaction, from each
95 dataset and trained models on the combined 70 % splits across all five datasets.

96 Our network outperformed eight of the most popular approaches for inferring gene-
97 regulatory relationships, including two deep convolutional neural networks[22,18] and six other
98 methods[8,23,24,25,26,27] (Fig. 1c). We measured the performance of the six methods across the
99 combined training and validation splits for each dataset, then compared the results with the cross-
100 validated performance of the deep learning-based methods on the held-out examples alone. With
101 one exception, the deep learning-based methods outperformed all others according to the areas

under both the precision-recall (PR) and receiver operating characteristic (ROC) curves. Moreover, DELAY outperformed all the other methods according to both metrics but performed slightly worse by area under the PR curve than by area under the ROC curve for the class-imbalanced embryonic datasets. Even though one of the deep learning-based methods, DeepDRIM, was trained on fivefold as many neighbor-gene matrices as DELAY, it still performed second- or third-best behind DELAY for all metrics. Together, these results suggest that DELAY outperforms the eight other methods because it learns important features from pseudotime-lagged gene-coexpression matrices.

Transfer learning allows DELAY to predict novel gene-regulatory networks from new single-cell datasets.

To test whether DELAY generalizes to new datasets, we examined the human hepatocyte (hHep) gene-regulatory network using an additional dataset with over four hundred single cells and known ground-truth interactions from ChIP-seq data[14,28]. We inferred the network by the previous methods and found that tree- and mutual information-based methods performed slightly better than deep learning-based methods, which performed comparably to random predictors (Fig. 1d). To determine whether this lack of generalizability arises from batch effects in the single-cell data, we used transfer learning to fine-tune the three deep learning-based methods on small fractions of the new dataset. After training each network on only 1 % of the new examples, their performance matched or exceeded that of the other methods, and training on up to 20 % of the examples yielded further performance increases. As observed previously, DELAY outperformed every other deep learning-based method. We did not observe any overfitting in the networks' fine-tuning curves for the mean validation metric, suggesting that the networks recognized general features of direct gene regulation associated with strong, well-optimized minima in the training loss. Moreover, these results demonstrate that DELAY can accurately predict gene-regulatory relationships from new datasets with partially known ground-truth labels.

127 **DELAY performs well with new input configurations, augmented matrices, and modified**
128 **datasets.**

129 Using different numbers of pseudotime-lagged gene-coexpression matrices or neighbor-gene
130 matrices, as well as examples from modified datasets with fewer cells or additional gene dropouts,
131 we next examined the performance of DELAY across various input configurations. We employed
132 the original datasets to train new cross-validated models on gene-coexpression matrices of up to
133 ten pseudotime lags (Fig. 2a) or up to ten neighbor genes (Supplementary Fig. 3), as well as on
134 gene-coexpression matrices with varying dimensions and resolutions. Training DELAY on at least
135 one pseudotime-lagged matrix or with at least one neighbor gene greatly increased the network's
136 performance across all datasets. Although training DELAY on up to ten pseudotime-lagged
137 matrices resulted in comparable or slightly better performance across all datasets, training the
138 network on more than two neighbor-gene matrices per gene decreased performance in some
139 instances. Adding channel masks for specific lagged matrices suggested that DELAY relies on
140 redundancies across all available lagged inputs (Supplementary Fig. 4).

141 We also characterized DELAY's performance on pseudotime-shuffled trajectories and
142 observed a sharp decrease in performance after reordering nearby cells in each trajectory (Fig. 2b).
143 This result suggests that the network relies heavily on the specific ordering of adjacent cells in
144 each trajectory. Upon examining DELAY's performance on modified datasets containing fewer
145 single cells (Fig. 2c) or additional gene-dropout noise (Fig. 2d), we also discovered that the
146 network was more sensitive to down-sampling of single cells than to gene-expression losses in
147 low-expressing cells alone. These results indicate that DELAY relies more heavily on highly
148 expressing cells and therefore learns larger input weights for the first lagged input because on
149 average that input contains stronger features of gene activation than other lags (Figs. 2e,f). To
150 investigate this hypothesis, we used augmented input matrices with masked regions to show that
151 DELAY relies heavily on the combined upper-left, upper-right, and lower-right regions
152 ($A_{ON} \cup B_{ON}$) across all lagged matrices (Fig. 2g). By performing a *post hoc* analysis of the
153 statistical dispersion across correctly inferred gene-pair examples, we additionally found that

154 DELAY performs best on transcription factors with stable gene expression along single-cell
155 trajectories (Supplementary Fig. 5).

156 **DELAY recognizes causal relationships in higher-order and cyclic gene-regulatory**
157 **interactions.**

158 To further investigate how the selection of neighbor genes can alter DELAY's internal
159 representations and subsequent gene-regulatory inferences, we modified gene-pair examples to
160 exclude all neighbor genes with known higher-order interactions across several classes of three-
161 gene motifs. First, we used DELAY to infer gene regulation across several classes of potential
162 higher-order interactions (Fig. 3a), including mutual interactions (MIs), feedback loops (FBLs),
163 and three classes of feedforward loops (FFLs). Unlike ordinary Granger causality, DELAY
164 performs well across cyclic interactions including 2-cycles (MIs) and 3-cycles (FBLs), which are
165 ubiquitous among gene-regulatory networks[29]. We next excluded all input matrices for neighbor
166 genes involved in potential FBLs and FFLs to ascertain how DELAY performs in their absence.
167 Because we saw a significant decrease in performance upon excluding these neighbors in most
168 cases of shared and sequential regulation but not downstream targets, DELAY apparently
169 recognizes the differences between input matrices of causally related genes and those of merely
170 correlated genes. Moreover, these results suggest that although our network uses principles of
171 Granger causality, it can achieve true causal inference for genes involved in several classes of
172 higher-order and cyclic regulatory interactions by avoiding several limiting assumptions of
173 ordinary Granger causality.

174 **DELAY performs best on zinc-finger proteins, bHLH factors, and other chromatin**
175 **remodelers.**

176 To explore how DELAY performs on classes of transcription factors containing different types of
177 DNA-binding domains, we analyzed the enrichment of gene-ontology (GO) terms across correctly
178 inferred transcription factors (Fig. 3b). We found that DELAY performs best on zinc-finger
179 proteins, bHLH factors, and other chromatin remodelers. Although DELAY performs well on

180 C2H2-type zinc-finger proteins in terms of the total number of correct predictions, we found that
181 it performs better on other chromatin remodelers and plant homeodomain (PHD) zinc-finger
182 proteins by the overall term enrichment. Interestingly, these results indicate that training the
183 network on cell type-specific ChIP-seq data allows the network to identify regulatory relationships
184 involving some non-sequence-specific transcription factors and cofactors that nevertheless
185 associate with specific targets at preferred chromatin conformations (Supplementary Table 1).

186 **Predicting the gene-regulatory network of auditory hair cells through multi-omic transfer**
187 **learning.**

188 We next sought to generate predictions for a cell type with complex but incompletely characterized
189 gene-regulatory dynamics. We devised a pipeline for multi-omic transfer learning to infer the
190 gene-regulatory network for developing mouse outer hair cells (mOHCs), the mechanical
191 amplifiers of the inner ear. We used both gene-expression[30] and chromatin-accessibility[31] datasets
192 to fine-tune our network. By first calculating the cell-by-gene accessibility scores across annotated
193 genes, we were able to generate lagged input matrices for the scATAC-seq dataset (Fig. 4a).
194 Because the underlying gene-expression and gene-accessibility distributions are both zero-
195 inflated[8], the resulting coaccessibility matrices are qualitatively similar to gene-coexpression
196 matrices.

197 To determine whether pseudotime-lagged gene-coaccessibility matrices contain features
198 that indicate direct gene-regulatory relationships, we fine-tuned DELAY on the scATAC-seq
199 matrices using available ground-truth examples collected from two cell type-specific datasets of
200 Sox2 and Atoh1 target genes[32,33]. Seventy percent of the ground-truth examples were used for fine-
201 tuning, and the remaining 30 % were held out for validation (Fig. 4b). DELAY again performed
202 slightly worse by the metric of area under the PR curve than by area under the ROC curve,
203 indicating that the network is better at discriminating false positives than selecting true positives.
204 Although DELAY did not outperform all other deep learning-based methods, the network's
205 performance was comparable to previous training on small fractions of the hHep scRNA-seq

206 dataset, which suggests that gene-coaccessibility matrices are also useful for inferring direct gene-
207 regulatory interactions.

208 Given that DELAY is well-optimized and benefits from additional training examples, we
209 separately fine-tuned the network on all available Sox2 and Atoh1 ground-truth examples from an
210 additional mOHC gene-expression dataset[30]. With previously determined hyperparameters for
211 scRNA-seq data, training DELAY on two GPUs required 230 ± 1 min (mean ± SD) per cross-
212 validated model. We then compared the target gene-rank correlations between the inferred
213 transcription factor-only gene-regulatory networks to determine whether networks inferred from
214 scRNA-seq data and scATAC-seq data were similar (Fig. 4c). Although we observed stronger
215 correlations between predictions from dataset-specific, cross-validated models than between
216 average predictions across datasets, the target gene-rank correlations between the two datasets
217 were highly variable and the predictions of some transcription factors agreed better than others.
218 Reasoning that the inferences with better agreement across datasets constituted the best predictions
219 and highest-confidence interactions, we derived the consensus hair cell gene-regulatory network
220 from the average predictions across both datasets. The resulting network consisted of 347 predicted
221 transcription factor-target gene interactions with regulation probabilities greater than 0.5.

222 **DELAY identifies important genes, interactions, and modules in the hair cell gene-**
223 **regulatory network.**

224 We used hierarchical clustering to group transcription factors and target genes in the transcription
225 factor-only gene-regulatory network for hair cells by similarities in their predicted targets and
226 regulators, respectively (Fig. 4d). This procedure revealed two distinct developmental modules
227 corresponding to prosensory genes such as *Sox2*, *Id2*, *Hes1*, and *Prox1* and hair cell genes such as
228 *Atoh1*, *Pou4f3*, *Gfi1*, *Lhx3*, and *Barhl1*. We sought to validate the predicted interactions by
229 comparing the locations of known transcription factor-binding sites[34,35] to the locations of open-
230 chromatin peaks[31] within 50 kb of target genes' transcription start sites. Twenty-two of 28
231 predicted interactions were confirmed by the accessibility of transcription-factor binding sites. Of

232 the six remaining interactions, three were instances of predicted target-gene regulation by
233 transcriptional cofactors lacking true DNA-binding domains. We additionally identified 13
234 reported interactions that were not detected by DELAY[31,36,37,38,39,40,41,42,43,44,45,46,47,48,49,50,51,52,53,54].
235 The most notable feature of the inferred gene-regulatory network for hair cells is that *Sox2*
236 and *Id2*—in addition to the well-known roles of their products in the maintenance of a prosensory-
237 cell fate and the regulation of target genes—are themselves the targets of a wide variety of
238 transcription factors including Sox proteins, homeobox factors, zinc-finger proteins, and Notch
239 effectors. Eleven of the 22 interactions confirmed by our binding-site accessibility analysis
240 represented direct regulation of *Sox2* and *Id2*, including mutually activating interactions between
241 *Sox2* and *Sox9*, *Sox11*, *Prox1*, and *Hes1*, and mutual inhibition with *Hist1h1c*. One other study has
242 suggested that Hes1 directly regulates *Sox2*[55].
243 Another notable feature of the inferred hair cell network is that the LIM-homeobox
244 transcription factor Lhx3 regulates its own expression as well as that of two other LIM-only
245 transcription factors (Lmo4 and Lmo1). This result implies a role for Lhx3 in maintaining the later
246 expression of these important early *Sox2* inhibitors[31,47,49]. Other key features of the network
247 include *Sox11* regulation by Hes1, *Nfkbia* regulation by Gfi1, and regulation of the splicing-factor
248 gene *Srsf2* by the products of three different prosensory genes. Srsf2 was recently predicted to play
249 a role in the splicing of an important deafness gene in humans[56].

250 **Discriminative motif analysis of target-gene enhancer sequences enables *de novo* discovery**
251 **of DNA-binding motifs.**

252 DELAY permits a complementary approach to typical gene-regulatory inference workflows such
253 as SCENIC[57] that use *cis*-regulatory sequences to identify and discard false-positive interactions
254 resulting from indirect gene regulation[11,30,31]. Because these methods rely on databases of known
255 DNA-binding motifs, they necessarily overlook predictions for cofactors and putative transcription
256 factors with unknown binding sequences. Instead of using *cis*-regulatory sequences to refine our
257 initial predictions, we introduced enhancer-sequence information *post hoc* to perform

258 discriminative motif analysis within the enhancers of predicted target genes in the hair cell network
259 (Fig. 5a, Supplementary Fig. 6). Notably, we identified enriched motifs that closely resembled
260 known DNA-binding motifs for nine of eleven transcription factors with at least one predicted
261 target gene in the transcription factor-only hair cell network (Supplementary Table 2).

262 We additionally sought to predict the mechanisms by which several identified hair cell
263 cofactors accomplish sequence-specific gene regulation in the absence of true DNA-binding
264 domains. Specifically, we compared sequences enriched in the enhancers of cofactors' predicted
265 targets to several databases of known DNA-binding motifs to identify the cofactors' DNA-binding
266 partners (so-called "guilt by association"). Through this analysis, we were able to determine that
267 the most significantly enriched sequence in the enhancers of the histone Hist1h1c's predicted target
268 genes closely matched known binding motifs for several SoxB2/A transcription factors (Fig. 5b).
269 In addition, a sequence enriched in the enhancers of cyclin Ccnd1's targets closely matched known
270 motifs for the Pbx family of homeobox transcription factors (Supplementary Fig. 7). These
271 cofactors might form complexes with the identified transcription factors to regulate their target
272 genes in hair cells.

273 As a final demonstration of DELAY's high-confidence predictions, we used the fine-tuned
274 scRNA-seq models to generate regulatory predictions for transcription factors expressed in at least
275 20 % of developing hair cells (Supplementary Table 3). After considering these additional
276 transcription factors, we identified the putative C2H2 zinc-finger protein Fiz1 as a likely regulator
277 of *Sox2* and *Hes6*. Discriminative motif analysis of these genes' enhancer sequences (Fig. 5c)
278 uncovered a likely Fiz1 consensus DNA-binding sequence (5'-CGCTGC-3') similar to that of other
279 *Sox2* regulators from the Zic family of C2H2 zinc-finger proteins[58].

280 Discussion

281 Building upon several deep learning-based methods[18,22], we have demonstrated that combining
282 fully-supervised deep learning with joint-probability matrices of pseudotime-lagged single-cell
283 trajectories can overcome certain limitations of current Granger causality-based methods of gene-

284 regulatory inference[9,12], such as their inability to infer cyclic regulatory motifs. Moreover, although
285 our convolutional neural network DELAY remains sensitive to the ordering of single cells in
286 pseudotime, the network can accurately infer direct gene-regulatory interactions from both
287 timecourse and snapshot datasets, unlike many supervised methods that rely strongly on the
288 number of available time-course samples[15,16]. We suspect that DELAY is sensitive to the specific
289 ordering of adjacent cells in trajectories because pseudotime inference methods such as Slingshot[6]
290 infer lineages from minimum spanning trees that directly depend on cell-to-cell similarities in
291 gene-expression values[7].

292 We have presented a multi-omic paradigm for fine-tuning DELAY on both gene-
293 expression and chromatin-accessibility datasets for the development of auditory hair cells. The
294 network's accurate predictions allowed *de novo* inferences of known and unknown DNA-binding
295 motifs, establishing DELAY as a complementary approach to common methods of gene-
296 regulatory inference. Our method's high-confidence predictions across the hair cell gene-
297 regulatory network also support it as an attractive option for experimentalists with limited
298 resources to predict true gene-regulatory relationships from complex, large-scale gene-regulatory
299 networks while avoiding spurious, indirect interactions often introduced through unsupervised
300 methods[14].

301 We have additionally identified with high confidence interactions between cofactors and
302 target genes in the regulatory network of hair cells that methods such as SCENIC[57] would have
303 overlooked. Using "guilt by association," we predicted that the cyclin Ccnd1—a known
304 transcriptional cofactor found at the enhancers of several *Id* genes during retinal development[59]—
305 forms complexes with the Pbx family of homeobox transcription factors, of which at least one is a
306 known target of Prox1 in the inner ear[60]. Moreover, we predicted that the retina-specific linker
307 histone Hist1h1c[61] forms complexes with the SoxB2 family of transcription factors, which have
308 known antagonistic effects on *Sox2* expression in hair cells[62]. Finally, we predicted that the
309 putative hair cell-specific C2H2 zinc-finger protein Fiz1—which is also expressed during retinal

310 development[63]—is a regulator of *Sox2* in hair cells and identified its likely DNA-binding sequence
311 in the enhancers of predicted target genes.

312 Believing that DELAY will be a valuable resource to the community, we have provided an
313 open-source implementation of the algorithm as well as pre-trained model weights for subsequent
314 fine-tuning on new single-cell datasets and partial ground-truth labels. Although we chose to fine-
315 tune DELAY on cell type-specific ChIP-seq data, future studies may choose to fine-tune DELAY
316 on curated interactions from databases or from gain- or loss-of-function experiments, especially in
317 the absence of ChIP-seq data[14]. These additional interactions can also supplement smaller ground-
318 truth datasets, such as those of Sox2 and Atoh1 target genes, to mitigate false-negative predictions.
319 We believe the modest computational cost of training new models of DELAY will prove a
320 worthwhile investment for future investigations into complex gene-regulatory networks.

321 Methods

322 Preparing single-cell RNA-seq datasets to train and test the convolutional neural network.

323 To train our convolutional neural network, we used scRNA-seq datasets from two timecourse
324 studies of endodermal specification of human embryonic stem cells[19] and mouse embryonic stem
325 cells[20] and an *in vivo* snapshot study of erythroid (E), granulocyte-monocyte (GM), and lymphoid
326 (L) specification in mouse hematopoietic stem cells[21]. We additionally employed a dataset from a
327 timecourse study of the differentiation of human hepatocytes from induced pluripotent stem cells
328 to test our network[28]. For each of these studies, we collected the normalized gene-expression
329 values, pseudotime values, and ground-truth networks from BEELINE's supplementary data
330 files[14,64]. In BEELINE, Pratapa *et al*. collected the normalized gene-expression values from the
331 original studies or obtained the values themselves by log-transforming the transcripts per kilobase
332 million. Moreover, those authors used Slingshot[6] to infer the pseudotime values separately for each
333 dataset, orienting the inferred trajectories by known experimental timepoints or precursor-cell
334 types and lineages. Finally, Pratapa *et al*. selected genes with differential expression across
335 pseudotime by applying generalized additive models (GAMs) to compute gene variances and their

associated P values. To train DELAY, we utilized their gene variances and corrected P values to select differentially expressed transcription factors ($P_{\text{adjusted}}<0.01$) and 500 additional genes with the highest variance for each dataset. We also collected the ground-truth labels from BEELINE's supplementary data files, which contained tables of transcription factor-target gene interactions curated from cell type-specific ChIP-seq experiments in the ENCODE[65], ChIP-Atlas[66], and ESCAPE[67] databases. Table 1 provides details for each dataset including descriptions of the ground-truth networks.

We also characterized our network on modified datasets with shuffled pseudotime, fewer cells, and additional gene-dropout noise. We shuffled pseudotime values across single-cell trajectories using the np.random.normal function in NumPy (v1.20.2) to select the indices of single cells either leading or lagging successive cells in each trajectory at some length scale σ before swapping the cells' positions in pseudotime. We used np.random.choice in NumPy to select the indices of single cells to retain when down-sampling the number of cells in a dataset. Lastly, we induced additional gene-dropout noise in datasets by setting the gene-expression values to zero with a probability of p for the bottom p percent of cells expressing each gene in a given dataset.

Generating examples of transcription factor-target gene pairs from single-cell datasets.

For each dataset, we generated mini-batches of 512 transcription factor-target gene-pair examples by first enumerating all possible combinations of differentially expressed transcription factors and potential target genes—including both transcription factors and highly varying genes. We then generated aligned and pseudotime-lagged gene-coexpression matrices for up to five lags with the following configurations as separate input channels: transcription factor-target, transcription factor-transcription factor, target-target, transcription factor-neighbor (for two neighbors), and target-neighbor (for two neighbors). We concatenated the input channels for each example to form three-dimensional stacks of input matrices with dimensions $42\times32\times32$ (channels x height x width). For each gene, we used the np.correlate function in NumPy to select the transcription

factors with the highest absolute cross-correlation at a maximum offset of five pseudotime lags to use as neighbor genes. After preparing mini-batches for each dataset, we used different integer values to seed the random_split function in PyTorch (v1.8.1) to produce pseudorandom, reproducible training (70 %) and validation (30 %) splits across each dataset for cross validation.

We later used the same validation splits to characterize our network on augmented coexpression matrices and matrices generated from modified single-cell datasets. To augment gene-coexpression matrices, we masked either specific regions across all input channels, or entire input channels corresponding to specific pseudotime lags, by setting all of the relevant pixel values to zero. We replaced features after motif-specific neighbor-gene ablations by selecting new highly correlated genes to replace neighbors involved in the higher-order gene-regulatory interactions.

Constructing a convolutional neural network to classify lagged gene-coexpression matrices.

We designed a convolutional neural network based on an inverted VGGnet[68] that uses five convolutional layers to first expand the input to 1024 channels, then successively halve the number of channels to 64 before classifying examples as either true regulation or no interaction with a fully-connected linear layer. Each convolutional layer sums over the two-dimensional cross-correlations ($\star$) of 3×3 kernels and input channels i to find the features for a given output channel j, as shown in Equation 1:

$$\text{output}\ (N_k, C_{\text{out}_j}) = \text{bias}\ (C_{\text{out}_j}) + \sum_{i=1}^{C_{\text{in}}} \text{weights}_{3\times3}(C_{\text{in}_i}, C_{\text{out}_j}) \star \text{input}\ (N_k, C_{\text{in}_i}), \qquad (1)$$

in which the weights and bias are trainable parameters, N is the mini-batch size, C is the number of channels, $C_{\text{out}} = C_{\text{in}}/2$ for layers two through five, and all convolutions are zero-padded at the edges of matrices. To preserve the gradient flow during training, we used leaky rectified linear units (ReLUs) with a negative slope of 0.2 (Equation 2) as our nonlinear activation function after each convolutional layer:

$$\text{Leaky ReLU}(x) = \max(0, x) + 0.2 * \min(0, x). \qquad (2)$$

As shown in Equation 3, we additionally used 2×2, unpadded max-pooling layers between convolutional layers to identify important features and down-sample activation maps:

$$\text{output}\ (N_k, C_{\text{out}_j}, \tfrac{h_{\text{in}}}{2}, \tfrac{w_{\text{in}}}{2}) = \underset{2\times 2}{\text{stride}}\ [\max_{m,n\,\in\,\{0,1\}} \text{input}\ (N_k, C_{\text{in}_j}, x_{m,n})], \tag{3}$$

in which x represents the 2×2 input windows and h, w are the height and width of the input channel j. After the final convolutional layer, we used global-average pooling (Equation 4) to reduce the remaining 64 feature maps j to a single, 64-dimensional latent vector x:

$$\text{output}\ (N_k, C_{\text{out}_j}) = \underset{h_{\text{in}}\times w_{\text{in}}}{\text{avg}}\ \text{input}\ (N_k, C_{in_j})\,. \tag{4}$$

We lastly used a fully-connected, linear layer (Equation 5) with a sigmoid activation function (Equation 6) to generate gene-regulation probabilities:

$$\text{output}\ (N_k) = \text{bias}_{\text{FC}} + \sum_{i=1}^{64} \text{weights}_{\text{FC}}\ (x_i) * \text{input}\ (N_k, x_i)\,, \tag{5}$$

$$\text{Sigmoid}(x) = \frac{1}{1+\exp(-x)}, \tag{6}$$

where a probability of $P > 0.5$ indicates a true gene-regulatory interaction for the given gene-pair example.

Training and fine-tuning the network on pseudotime-lagged gene-coexpression matrices.

We used PyTorch's implementation of stochastic gradient descent (SGD) to optimize our network with respect to the class-weighted binary cross-entropy loss, summed across each mini-batch and scaled by the overall batch size 512, as shown in Equation 7:

$$L(y, \hat{y}) = -\frac{w_N}{512}\sum_{n=1}^{N} y_n * \log \hat{y}_n + (1-y_n) * \log(1-\hat{y}_n)\,, \tag{7}$$

in which y and $\hat{y}$ are the target and predicted values (respectively), w_N is the fraction of true examples in the mini-batch, and N is the size of the current mini-batch (which might be less than 512). Prior to optimization, we used He initialization with uniform priors to set the weights for all convolutional and linear layers. We used a learning rate (LR) of 0.5 to train each model for up to

408 100 epochs, validating performance after each epoch, and stopping training after ten or more
409 epochs without an improvement in the average validation metric of areas under the curves.
410 For fine-tuning, we increased the LR and number of epochs over several orders of
411 magnitude when training models on smaller fractions of the testing dataset. To a lesser extent, we
412 also adjusted the LR and number of epochs when training models on different configurations of
413 lagged matrices, neighbor-gene matrices, and matrices of different sizes to improve training speed
414 and stability. When fine-tuning the network on scATAC-seq matrices, we used mini-batches with
415 24 examples each and trained for 50 to 100 epochs. We used two Nvidia RTX 8000 GPUs to train
416 each model.

417 **Comparing DELAY to other top-performing gene-regulatory inference methods.**

418 We compared the performance of our neural network to two other convolutional neural networks,
419 as well as the top six best-performing methods identified in a previous benchmarking study. Using
420 BEELINE, we inferred the gene-regulatory networks for all training and testing datasets using the
421 tree-based methods GENIE3[23] and GRNBoost2[24], the mutual information-based method PIDC[25],
422 and the partial-correlation and regression-based methods PPCOR[26], SCODE[27], and
423 SINCERITIES[8]. We utilized the best parameter values identified in BEELINE for the partial-
424 correlation and regression-based methods. For the two deep learning-based methods (CNNC[22] and
425 DeepDRIM[18]), we used the original studies to reconstruct the neural networks in PyTorch before
426 training five cross-validated models each. In addition to training both networks on pseudotime-
427 aligned gene-coexpression matrices for primary transcription factor-target gene pairs, we also
428 trained DeepDRIM on ten neighbor-gene matrices per gene. Neither network was trained on
429 pseudotime-lagged gene-coexpression matrices.

430 **Analyzing enrichment of gene-ontology terms across correctly inferred gene-pair examples.**

431 We used Enrichr[69] (https://maayanlab.cloud/Enrichr/) to analyze GO-term enrichment across
432 correctly inferred transcription factors for terms related to InterPro DNA-binding domains[70]. We

433 used a Fisher's exact test with Benjamini-Hochberg correction for multiple-hypothesis testing
434 ($P_{\text{adjusted}}<0.05$) to assess the statistical significance for each GO term.

435 **Preparing single-cell multi-omics datasets to infer the hair cell gene-regulatory network.**

436 We used two single-cell datasets from developing mouse outer hair cells[30,31] to predict the
437 consensus hair cell gene-regulatory network. First, we collected the normalized gene-expression
438 values from the original scRNA-seq study[30], then used reciprocal PCA to integrate single cells
439 across four timepoints of sensory-epithelium development into a single dataset in Seurat[71] (v3.1.4).
440 Then, we used Slingshot[6] (v1.0.0) to infer pseudotime values across the outer hair cell trajectory
441 and applied LOESS regressions and GAMs to select the genes that were differentially expressed
442 across both the sensory epithelium and pseudotime, respectively. We again selected all
443 differentially expressed transcription factors ($P<0.01$ after Bonferroni correction for multiple-
444 hypothesis testing) and 500 additional genes with the highest variance, and we used the integrated
445 gene-expression assay in Seurat to generate the corresponding gene-coexpression matrices. In a
446 separate analysis, we broadened our selection criteria to encompass all genes that were
447 differentially expressed in at least 20 % of the outer hair cells, regardless of their expression across
448 the full sensory epithelium.

449 For the scATAC-seq dataset, we first collected the cell-by-peak chromatin-accessibility
450 data from the original study[31]. Then, we used the function `createGmatFromMat` in SnapATAC[72]
451 (v1.0.0) to calculate the cell-by-gene accessibility scores as the counts of each 5 kb bin per gene
452 in the UCSC mouse genome mm10[73] (`TxDb.Mmusculus.UCSC.mm10.knownGene`; v3.4.4) that
453 contained at least one open-chromatin peak for a given cell. These values were then log-
454 normalized. We again used Slingshot to infer pseudotime values across the outer hair cell trajectory
455 and applied GAMs to the raw accessibility counts to select the differentially accessible genes
456 across pseudotime. For the inferred scATAC-seq network, we selected all differentially accessible
457 transcription factors and variable genes ($P_{\text{adjusted}}<0.01$) that were also differentially expressed
458 along the scRNA-seq trajectory. Because the scATAC-seq dataset had fewer single cells than the

459 scRNA-seq dataset, we used 24 fixed-width bins in each dimension to generate the corresponding
460 gene-coaccessibility matrices prior to fine-tuning.

461 **Discriminative motif analysis to discover *de novo* transcription factor binding motifs.**

462 We used the UCSC mouse genome mm10 and twoBitToFa to download the 100 kb enhancer
463 sequences spanning 50 kb upstream and downstream of all target genes' transcription start sites in
464 the transcription factor-only hair cell gene-regulatory network, then divided them into 100 bp
465 fragments and sorted the resulting sequences into primary (predicted targets) and control
466 (predicted no interaction) groups for each transcription factor with at least one target gene in the
467 network. We then used STREME[74] (v5.4.1) to perform discriminative motif analysis with a P
468 value threshold of 0.05 to identify enriched motifs in predicted target genes' enhancers, which we
469 then compared to either the transcription factors' known binding motifs from CIS-BP[34], or to all
470 motifs from the JASPAR[75], UniPROBE[76] (mouse), and Jolma et al. (2013)[77] databases using
471 TOMTOM[78] (v5.4.1) with an E value threshold of 10 for significant alignments.

472 ## Data availability

473 The processed experimental files for all single-cell datasets used in this study are available on
474 Zenodo at https://doi.org/10.5281/zenodo.5711739; Table 1 lists the Gene Expression Omnibus
475 (GEO) accession numbers for each dataset. The saved model weights for DELAY are available on
476 Zenodo at https://doi.org/10.5281/zenodo.5711792. All experimental logs from this study are
477 available at https://tensorboard.dev/experiment/RBVBetLMRDiEvO7sBl452A.

478 ## Code availability

479 We have provided an open-source implementation of DELAY in PyTorch with listed requirements
480 and documentation at https://github.com/calebclayreagor/DELAY.

Acknowledgements

The authors would like to acknowledge Junyue Cao, Viviana Risca, Christina Leslie, Adrian Jacobo, Agnik Dasgupta, Emily Atlas, and other members of the Laboratory of Sensory Neuroscience for helpful discussions and comments on the manuscript. C.C.R. is supported by National Science Foundation Graduate Research Fellowship Grant No. 1946429. A.J.H is an Investigator of Howard Hughes Medical Institute.

Author contributions

C.C.R. and N.V. conceived the study, and all authors designed the analysis. C.C.R. carried out all experiments and analysis and wrote the paper. A.J.H. supervised the project, and all the authors edited the paper.

Competing interests

The authors declare no competing interests.

References

1. Ocone, A., Haghverdi, L., Mueller, N. S. & Theis, F. J. Reconstructing gene regulatory dynamics from high-dimensional single-cell snapshot data. *Bioinformatics* **31**, i89–i96 (2015).
2. Qian, J., Dolled-Filhart, M., Lin, J., Yu, H. & Gerstein, M. Beyond synexpression relationships: local clustering of time-shifted and inverted gene expression profiles identifies new, biologically relevant interactions. *J. Mol. Biol.* **314**, 1053–1066 (2001).
3. Bar-Joseph, Z., Gitter, A. & Simon, I. Studying and modelling dynamic biological processes using time-series gene expression data. *Nat. Rev. Genet.* **13**, 552–564 (2012).
4. Ding, J., Sharon, N. & Bar-Joseph, Z. Temporal modelling using single-cell transcriptomics. *Nat. Rev. Genet.* (2022) doi:10.1038/s41576-021-00444-7.
5. Tritschler, S. *et al.* Concepts and limitations for learning developmental trajectories from single cell genomics. *Development* **146**, dev170506 (2019).
6. Street, K. *et al.* Slingshot: Cell lineage and pseudotime inference for single-cell transcriptomics. *BMC Genomics* **19**, 477 (2018).
7. Trapnell, C. *et al.* The dynamics and regulators of cell fate decisions are revealed by pseudotemporal ordering of single cells. *Nat. Biotechnol.* **32**, 381–386 (2014).
8. Papili Gao, N., Ud-Dean, S. M. M., Gandrillon, O. & Gunawan, R. SINCERITIES: Inferring gene regulatory networks from time-stamped single cell transcriptional expression profiles. *Bioinformatics* **34**, 258–266 (2018).
9. Deshpande, A., Chu, L.-F., Stewart, R. & Gitter, A. Network inference with Granger causality ensembles on single-cell transcriptomics. *Cell Rep.* **38**, 110333 (2022).

10. Finkle, J. D., Wu, J. J. & Bagheri, N. Windowed Granger causal inference strategy improves discovery of gene regulatory networks. *Proc. Natl. Acad. Sci.* **115**, 2252–2257 (2018).

11. Michailidis, G. & d'Alché-Buc, F. Autoregressive models for gene regulatory network inference: Sparsity, stability and causality issues. *Math. Biosci.* **246**, 326–334 (2013).

12. Zhang, Y., Chang, X. & Liu, X. Inference of gene regulatory networks using pseudo-time series data. *Bioinformatics* btab099 (2021) doi:10.1093/bioinformatics/btab099.

13. Qiu, X. *et al.* Inferring causal gene regulatory networks from coupled single-cell expression dynamics using scribe. *Cell Syst.* **10**, 265-274.e11 (2020).

14. Pratapa, A., Jalihal, A. P., Law, J. N., Bharadwaj, A. & Murali, T. M. Benchmarking algorithms for gene regulatory network inference from single-cell transcriptomic data. *Nat. Methods* **17**, 147–154 (2020).

15. Yuan, Y. & Bar-Joseph, Z. Deep learning of gene relationships from single cell time-course expression data. *Brief. Bioinform.* **22**, bbab142 (2021).

16. Xu, Y., Chen, J., Lyu, A., Cheung, W. K. & Zhang, L. *dynDeepDRIM: a dynamic deep learning model to infer direct regulatory interactions using single cell time-course gene expression data*. http://biorxiv.org/lookup/doi/10.1101/2021.08.28.458048 (2021) doi:10.1101/2021.08.28.458048.

17. Granger, C. W. J. Investigating causal relations by econometric models and cross-spectral methods. *Econometrica* **37**, 424–38 (1969).

18. Chen, J. *et al.* DeepDRIM: A deep neural network to reconstruct cell-type-specific gene regulatory network using single-cell RNA-seq data. *Brief. Bioinform.* **22**, (2021).

19. Chu, L.-F. *et al.* Single-cell RNA-seq reveals novel regulators of human embryonic stem cell differentiation to definitive endoderm. *Genome Biol.* **17**, (2016).

20. Hayashi, T. *et al.* Single-cell full-length total RNA sequencing uncovers dynamics of recursive splicing and enhancer RNAs. *Nat. Commun.* **9**, 619 (2018).

21. Nestorowa, S. *et al.* A single-cell resolution map of mouse hematopoietic stem and progenitor cell differentiation. *Blood* **128**, e20–e31 (2016).

22. Yuan, Y. & Bar-Joseph, Z. Deep learning for inferring gene relationships from single-cell expression data. *Proc. Natl. Acad. Sci.* **116**, 27151–27158 (2019).

23. Huynh-Thu, V. A., Irrthum, A., Wehenkel, L. & Geurts, P. Inferring regulatory networks from expression data using tree-based methods. *PLoS ONE* **5**, e12776 (2010).

24. Moerman, T. *et al.* GRNBoost2 and Arboreto: Efficient and scalable inference of gene regulatory networks. *Bioinformatics* **35**, 2159–2161 (2019).

25. Chan, T. E., Stumpf, M. P. H. & Babtie, A. C. Gene regulatory network inference from single-cell data using multivariate information measures. *Cell Syst.* **5**, 251-267.e3 (2017).

26. Kim, S. ppcor: An R package for a fast calculation to semi-partial correlation coefficients. *Commun. Stat. Appl. Methods* **22**, 665–674 (2015).

27. Matsumoto, H. *et al.* SCODE: An efficient regulatory network inference algorithm from single-cell RNA-Seq during differentiation. *Bioinformatics* **33**, 2314–2321 (2017).

28. Camp, J. G. *et al.* Multilineage communication regulates human liver bud development from pluripotency. *Nature* **546**, 533–538 (2017).

29. Alon, U. Network motifs: theory and experimental approaches. *Nat. Rev. Genet.* **8**, 450–461 (2007).

558 30. Kolla, L. *et al.* Characterization of the development of the mouse cochlear epithelium at
559 the single cell level. *Nat. Commun.* **11**, 2389 (2020).

560 31. Wang, S., Lee, M. P., Jones, S., Liu, J. & Waldhaus, J. Mapping the regulatory landscape
561 of auditory hair cells from single-cell multi-omics data. *Genome Res.* gr.271080.120 (2021)
562 doi:10.1101/gr.271080.120.

563 32. Kwan, K. Y., Shen, J. & Corey, D. P. C-MYC transcriptionally amplifies SOX2 target
564 genes to regulate self-renewal in multipotent otic progenitor cells. *Stem Cell Rep.* **4**, 47–60
565 (2015).

566 33. Cai, T. *et al.* Characterization of the transcriptome of nascent hair cells and identification
567 of direct targets of the Atoh1 transcription factor. *J. Neurosci.* **35**, 5870–5883 (2015).

568 34. Weirauch, M. T. *et al.* Determination and inference of eukaryotic transcription factor
569 sequence specificity. *Cell* **158**, 1431–1443 (2014).

570 35. Grant, C. E., Bailey, T. L. & Noble, W. S. FIMO: scanning for occurrences of a given
571 motif. *Bioinformatics* **27**, 1017–1018 (2011).

572 36. Zheng, J. L., Shou, J., Guillemot, F., Kageyama, R. & Gao, W. Q. Hes1 is a negative
573 regulator of inner ear hair cell differentiation. *Development* **127**, 4551–4560 (2000).

574 37. Zine, A. *et al.* Hes1 and Hes5 activities are required for the normal development of the
575 hair cells in the mammalian inner ear. *J. Neurosci.* **21**, 4712–4720 (2001).

576 38. Ikeda, R., Pak, K., Chavez, E. & Ryan, A. F. Transcription factors with conserved
577 binding sites near ATOH1 on the POU4F3 gene enhance the induction of cochlear hair cells.
578 *Mol. Neurobiol.* **51**, 672–684 (2015).

579 39. Du, X. *et al.* Regeneration of mammalian cochlear and vestibular hair cells through
580 Hes1/Hes5 modulation with siRNA. *Hear. Res.* **304**, 91–110 (2013).

581 40. Kirjavainen, A. *et al.* Prox1 interacts with Atoh1 and Gfi1, and regulates cellular
582 differentiation in the inner ear sensory epithelia. *Dev. Biol.* **322**, 33–45 (2008).

583 41. Yu, K. S. *et al.* Development of the mouse and human cochlea at single cell resolution.
584 739680 (2019).

585 42. Benito-Gonzalez, A. & Doetzlhofer, A. Hey1 and Hey2 control the spatial and temporal
586 pattern of mammalian auditory hair cell differentiation downstream of hedgehog signaling. *J.*
587 *Neurosci.* **34**, 12865–12876 (2014).

588 43. Doetzlhofer, A. *et al.* Hey2 regulation by FGF provides a Notch-independent mechanism
589 for maintaining pillar cell fate in the Organ of Corti. *Dev. Cell* **16**, 58–69 (2009).

590 44. Kamaid, A., Neves, J. & Giraldez, F. Id gene regulation and function in the prosensory
591 domains of the chicken inner ear: A link between Bmp signaling and Atoh1. *J. Neurosci.* **30**,
592 11426–11434 (2010).

593 45. Yu, R., Wang, P. & Chen, X.-W. The role of gfi1.2 in the development of zebrafish inner
594 ear. *Hear. Res.* **396**, 108055 (2020).

595 46. Jones, J. M. Inhibitors of differentiation and DNA binding (Ids) regulate Math1 and hair
596 cell formation during the development of the Organ of Corti. *J. Neurosci.* **26**, 550–558 (2006).

597 47. Hertzano, R. *et al.* Lhx3, a LIM domain transcription factor, is regulated by Pou4f3 in the
598 auditory but not in the vestibular system. *Eur. J. Neurosci.* **25**, 999–1005 (2007).

599 48. Hertzano, R. *et al.* Transcription profiling of inner ears from Pou4f3 ddl/ddl identifies
600 Gfi1 as a target of the Pou4f3 deafness gene. *Hum. Mol. Genet.* **13**, 2143–2153 (2004).

601 49. Deng, M. *et al.* LMO4 functions as a negative regulator of sensory organ formation in the
602 mammalian cochlea. *J. Neurosci.* **34**, 10072–10077 (2014).

603 50. Bae, S., Bessho, Y., Hojo, M. & Kageyama, R. The bHLH gene Hes6, an inhibitor of
604 Hes1, promotes neuronal differentiation. *Development* **127**, 2933–2943 (2000).

605 51. Fior, R. & Henrique, D. A novel hes5/hes6 circuitry of negative regulation controls
606 Notch activity during neurogenesis. *Dev. Biol.* **281**, 318–333 (2005).

607 52. Matern, M. S. *et al.* GFI1 functions to repress neuronal gene expression in the developing
608 inner ear hair cells. *Development* **147**, dev186015 (2020).

609 53. Hou, K. *et al.* A critical E-box in Barhl1 3′ enhancer is essential for auditory hair cell
610 differentiation. *Cells* **8**, 458 (2019).

611 54. Chonko, K. T. *et al.* Atoh1 directs hair cell differentiation and survival in the late
612 embryonic mouse inner ear. *Dev. Biol.* **381**, 401–410 (2013).

613 55. Waldhaus, J. *et al.* Stemness of the Organ of Corti relates to the epigenetic status of Sox2
614 enhancers. *PLoS ONE* **7**, e36066 (2012).

615 56. Booth, K. T. *et al.* Novel loss-of-function mutations in COCH cause autosomal recessive
616 nonsyndromic hearing loss. *Hum. Genet.* **139**, 1565–1574 (2020).

617 57. Aibar, S. *et al.* SCENIC: single-cell regulatory network inference and clustering. *Nat.*
618 *Methods* **14**, 1083–1086 (2017).

619 58. Marchal, L., Luxardi, G., Thomé, V. & Kodjabachian, L. BMP inhibition initiates neural
620 induction via FGF signaling and Zic genes. *Proc. Natl. Acad. Sci.* **106**, 17437–17442 (2009).

621 59. Bienvenu, F. *et al.* Transcriptional role of cyclin D1 in development revealed by a
622 genetic–proteomic screen. *Nature* **463**, 374–378 (2010).

623 60. Luo, Z., Zhang, J., Qiao, L., Lu, F. & Liu, Z. Mapping genome-wide binding sites of
624 Prox1 in mouse cochlea using the CUT&RUN approach. *Neurosci. Bull.* **37**, 1703–1707
625 (2021).

626 61. Popova, E. Y. *et al.* Developmentally regulated linker histone H1c promotes
627 heterochromatin condensation and mediates structural integrity of rod photoreceptors in
628 mouse retina. *J. Biol. Chem.* **288**, 17895–17907 (2013).

629 62. Freeman, S. D. & Daudet, N. Artificial induction of Sox21 regulates sensory cell
630 formation in the embryonic chicken inner ear. *PLoS ONE* **7**, e46387 (2012).

631 63. Mali, R. S. *et al.* FIZ1 is part of the regulatory protein complex on active photoreceptor-
632 specific gene promoters in vivo. *BMC Mol. Biol.* **9**, 87 (2008).

633 64. Pratapa, A., Amogh Jalihal, Law, J., Bharadwaj, A., & T M Murali. Benchmarking
634 algorithms for gene regulatory network inference from single-cell transcriptomic data. (2020)
635 doi:10.5281/ZENODO.3701939.

636 65. The ENCODE Project Consortium. An integrated encyclopedia of DNA elements in the
637 human genome. *Nature* **489**, 57–74 (2012).

638 66. Oki, S. *et al.* ChIP-Atlas: A data-mining suite powered by full integration of public ChIP-
639 seq data. *EMBO Rep.* **19**, (2018).

640 67. Xu, H., Ang, Y.-S., Sevilla, A., Lemischka, I. R. & Ma'ayan, A. Construction and
641 validation of a regulatory network for pluripotency and self-renewal of mouse embryonic stem
642 cells. *PLoS Comput. Biol.* **10**, e1003777 (2014).

643 68. Simonyan, K. & Zisserman, A. Very deep convolutional networks for large-scale image
644 recognition. in (2015). doi:arXiv:1409.1556v6.

645 69. Kuleshov, M. V. *et al.* Enrichr: a comprehensive gene set enrichment analysis web server
646 2016 update. *Nucleic Acids Res.* **44**, W90–W97 (2016).

70. Blum, M. *et al.* The InterPro protein families and domains database: 20 years on. *Nucleic Acids Res.* **49**, D344–D354 (2021).

71. Stuart, T. *et al.* Comprehensive integration of single-cell data. *Cell* **177**, 1888-1902.e21 (2019).

72. Fang, R. *et al.* Comprehensive analysis of single cell ATAC-seq data with SnapATAC. *Nat. Commun.* **12**, 1337 (2021).

73. Navarro Gonzalez, J. *et al.* The UCSC Genome Browser database: 2021 update. *Nucleic Acids Res.* **49**, D1046–D1057 (2021).

74. Bailey, T. L. STREME: accurate and versatile sequence motif discovery. *Bioinformatics* **37**, 2834–2840 (2021).

75. Khan, A. *et al.* JASPAR 2018: update of the open-access database of transcription factor binding profiles and its web framework. *Nucleic Acids Res.* **46**, D260–D266 (2018).

76. Hume, M. A., Barrera, L. A., Gisselbrecht, S. S. & Bulyk, M. L. UniPROBE, update 2015: new tools and content for the online database of protein-binding microarray data on protein–DNA interactions. *Nucleic Acids Res.* **43**, D117–D122 (2015).

77. Jolma, A. *et al.* DNA-binding specificities of human transcription factors. *Cell* **152**, 327–339 (2013).

78. Gupta, S., Stamatoyannopoulos, J. A., Bailey, T. L. & Noble, W. Quantifying similarity between motifs. *Genome Biol.* **8**, R24 (2007).

667 ## Tables and table legends

Datasets					Networks				
Cell Type	**TC/S**	**GEO**	**Set**	**Cells**	**TFs**	**Targets**	**Examples**	**Edges**	**Density**
hESC	TC	GSE75748	Train	758	37 (4)	541	20,017	3,166	15.82%
mESC	TC	GSE98664	Train	421	125 (17)	642	80,250	20,580	25.64%
mHSC -E	S	GSE75748	Train	1,071	33	533	17,589	9,592	54.53%
-GM	S	GSE75748	Train	889	23	523	12,029	6,587	54.76%
-L	S	GSE75748	Train	847	16	516	8,256	4,026	48.76%
hHep	TC	GSE81252	Test	425	33 (3)	536	17,688	6,171	34.89%
mOHC -scRNA	TC	GSE137299	Eval	1,563	56	556	1,112*	166*	14.93%*
-scATAC	S	GSE157398	Eval	391	48	382	764*	157*	20.55%*

668

669 **Table 1: Summary of the datasets used to train, test, and evaluate the neural network.**
670 Columns to the left (Cell Type to Cells) describe the single-cell datasets used to train, test, and
671 evaluate DELAY, and columns to the right (TFs to Density) describe the resulting gene-regulatory
672 networks, given the selected transcription factors and target genes. For three of the networks,
673 differentially-expressed transcription factors without target genes (in parentheses) were included
674 in our analysis as target genes, but not as transcription factors. All transcription factors were also
675 included as target genes, and gene-pair examples included all transcription factor-target gene pairs,
676 including examples of both true regulation (Edges, from ChIP-seq ground-truth data) and no
677 interaction. Gene Expression Omnibus (GEO) accession numbers are listed for each dataset.
678 Where indicated (*), network descriptions refer to partial ground-truth networks. hESC, human
679 embryonic stem cell; mESC, mouse embryonic stem cell; mHSC, mouse hematopoietic stem cell;
680 E, erythroid lineage; GM, granulocyte-monocyte lineage; L, lymphoid lineage; hHep, human
681 hepatocyte; mOHC, mouse outer hair cell; TC, time course; S, snapshot; TF, transcription factor.
682

Figures and figure legends

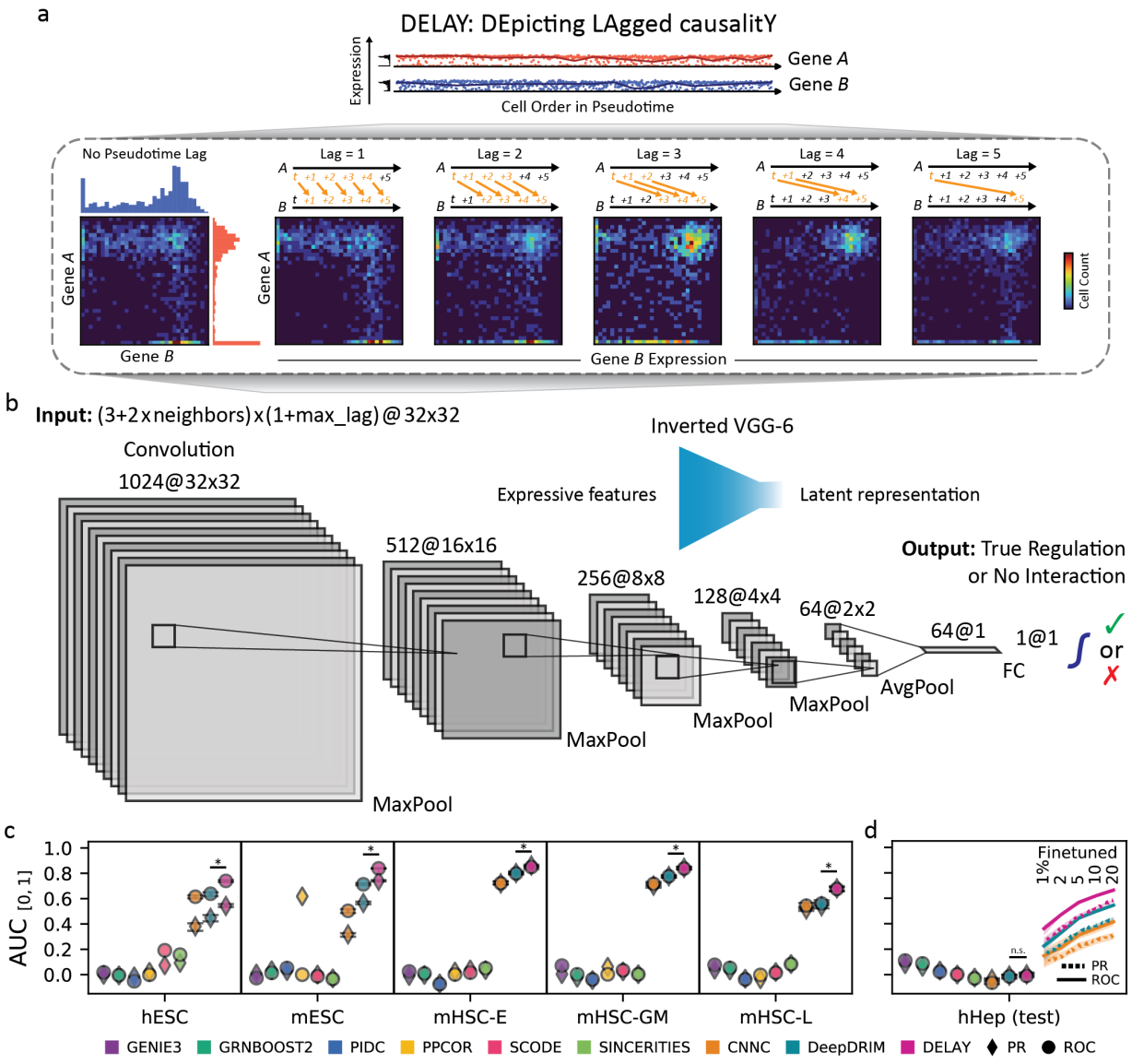

Figure 1: Pseudotime-lagged causality allows accurate inference of gene-regulatory networks.

a. Shifting the gene-expression trajectory of transcription factor *A* forward in pseudotime with respect to that of target gene *B* generates a series of unique joint-probability distributions. The resulting joint-probability matrices contain gene-coexpression signatures—in the upper-left, upper-right, and lower-right regions—that indicate *A* directly regulates *B*. **b.** The inverted architecture of DELAY is wide at the beginning of the network and progressively narrows to a

latent space followed by a linear classifier and sigmoid activation function to generate gene-regulation probabilities. The network uses leaky ReLU activations and padded 3x3 convolutions throughout. **c.** When trained on five benchmark scRNA-seq datasets, DELAY outperforms eight of the most popular methods for inferring gene-regulatory interactions. **d.** DELAY does not immediately generalize to a new testing dataset but outperforms all other methods if fine-tuned on a small percentage of the new data. The error bars and markers in **c** and **d** show the full range and average performance for each neural network across five cross-validated models. The values for areas under curves are normalized between a random predictor and perfect performance. The statistical significance between DELAY and the next-best neural network was assessed using a one-sided Wilcoxon signed-rank test (*, $P \leq 0.05$). PR, precision-recall; ROC, receiver operating characteristic.

Figure 2: The neural network relies on cell order in pseudotime and gene-expression strength.

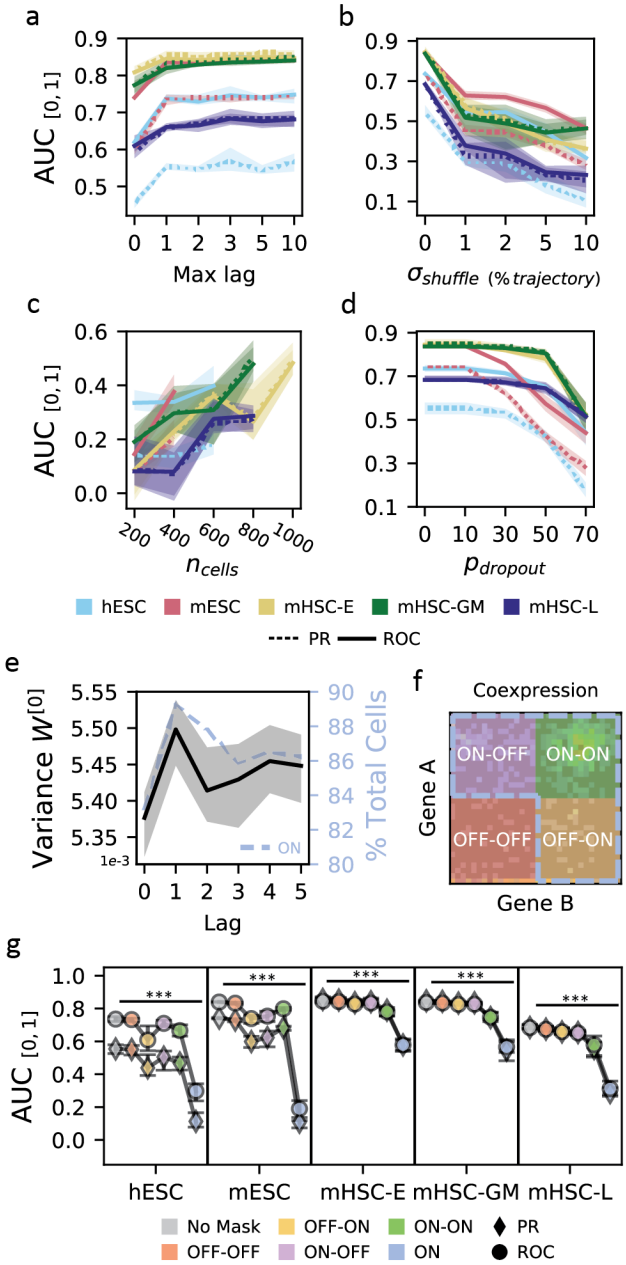

a. Training new models of DELAY on increasing numbers of pseudotime-lagged matrices gives the largest performance increase when using up to a single lag. **b.** Reordering single cells in pseudotime sharply decreases performance, suggesting that DELAY relies on the specific ordering of adjacent cells in each trajectory. **c, d.** The network is sensitive to random down-sampling of cells across datasets (**c**) but relatively more robust to induced, additional gene dropouts in weakly-expressing cells (**d**), suggesting DELAY relies heavily on highly-expressing cells. **e, f.** The network learns larger input weights for lagged matrices of the first pseudotime lag (**e**), which also contain on average more cells in the combined "ON" region ($A_{ON} \cup B_{ON}$; blue dotted outline, **f**) across training datasets (blue dotted line, **e**). The combined "ON" region is comprised of the upper-left "ON-OFF" quadrant ($A_{ON} \cap B_{OFF}$; purple, **f**), upper-right "ON-ON" quadrant ($A_{ON} \cap B_{ON}$; green, **f**), and lower-right "OFF-ON" quadrant ($A_{OFF} \cap B_{ON}$; yellow, **f**). **g.** Masking different regions of the input matrices shows that the network relies heavily on the combined "ON" region. Error bars and markers in **a-e** and **g** show the full range and average values across five cross-validated models. The statistical significance in **g** was assessed with a Kruskal-Wallis test (***, $P \leq 0.001$).

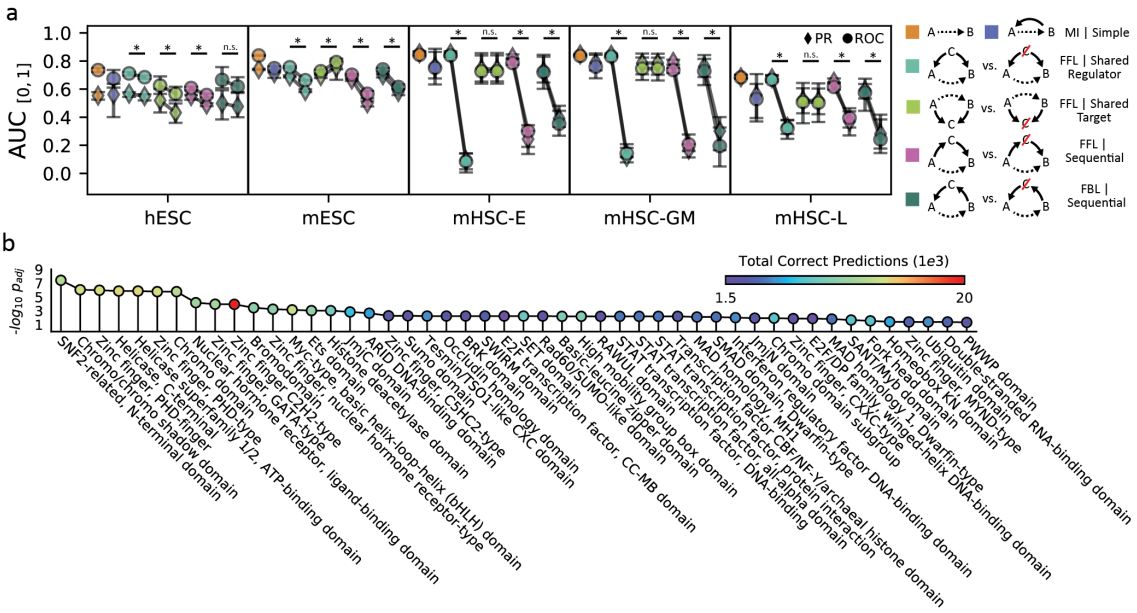

732

733 **Figure 3: DELAY uncovers causal, cyclic, and context-specific gene-regulatory relationships.**
734 **a.** The performance of the network on putative pairs of transcription factors and target genes
735 (dashed lines, legend) in two- and three-gene motifs with additional, known regulatory
736 relationships (solid lines, legend) suggests that DELAY distinguishes between various types of
737 higher-order and cyclic gene regulation. Upon exclusion of neighbor gene *C* from the input
738 features, performance declines significantly in cases of shared and sequential regulation (cyan and
739 pink/teal, respectively) but not for shared downstream targets (lime). **b.** Gene ontology-term
740 enrichment indicates that DELAY performs best on zinc-finger proteins (PHD-type, GATA-type,
741 C2H2-type, NHR-type, C5HC2-type), bHLH factors (Myc-type), and other chromatin remodelers
742 (SNF2-related, chromo domain, bromodomain, HDA domain, helicase). Error bars and markers in
743 **a** show the full range and average performance across five cross-validated models. The statistical
744 significance in **a** was assessed with a one-sided Wilcoxon signed-rank test (*, $P \leq 0.05$) and in **b**
745 with a Fisher's exact test ($P_{\text{adjusted}} < 0.05$). MI, mutual interaction; FFL, feedforward loop; FBL,
746 feedback loop.

747

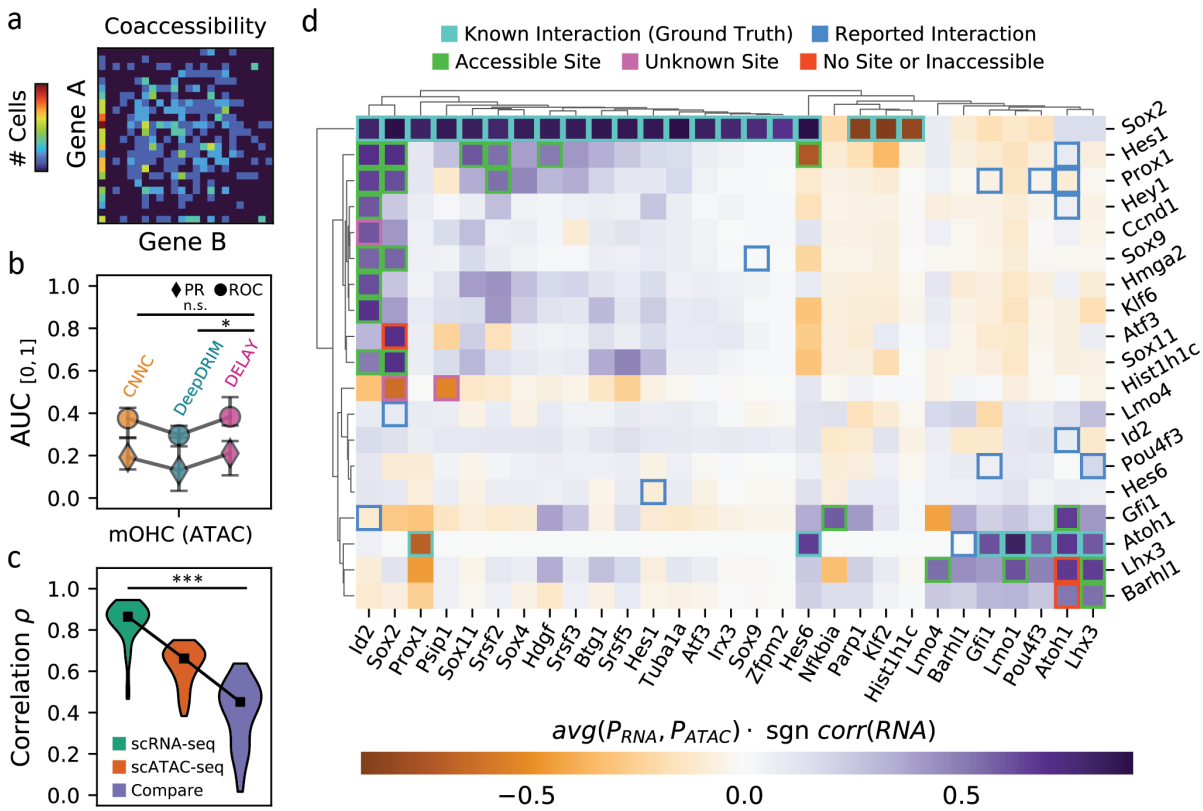

Figure 4: DELAY accurately predicts gene-regulatory interactions in the auditory hair cell network through multi-omic transfer learning.

a. An example of an empirical joint-probability matrix from scATAC-seq trajectories. **b.** After fine-tuning the network on lagged scATAC-seq input matrices, DELAY performs comparably to other neural networks and to previous testing on hHep scRNA-seq data. **c.** Training DELAY separately on scRNA-seq and scATAC-seq datasets of hair cell development reveals a stronger correlation between predictions from cross-validated models (green and orange) than between datasets (purple) across the transcription factor-only network. **d.** Average gene-regulation probabilities *P* across the hair cell gene-regulatory network accurately predict interactions between transcription factors (rows) and targets (columns), when comparing known binding sites to open-chromatin peaks in the target genes' enhancer sequences. Hierarchical clustering with WPGMA reveals distinct gene modules for prosensory genes (*Sox2*, *Id2*, *Hes1*, *Prox1*) and hair cell genes (*Atoh1*, *Pou4f3*, *Gfi1*, *Lhx3*, *Barhl1*). Up- or down-regulation was deduced from the correlation in the gene-expression data. Error bars and markers in **b** show the full range and average performance

763 for each neural network across five cross-validated models. Markers in **c** show the median target
764 gene-rank correlations across comparisons. The statistical significance in **b** was assessed with a
765 one-sided Wilcoxon signed-rank test (*, $P \leq 0.05$) and in **c** with a Kruskal-Wallis test (***,
766 $P \leq 0.001$).
767

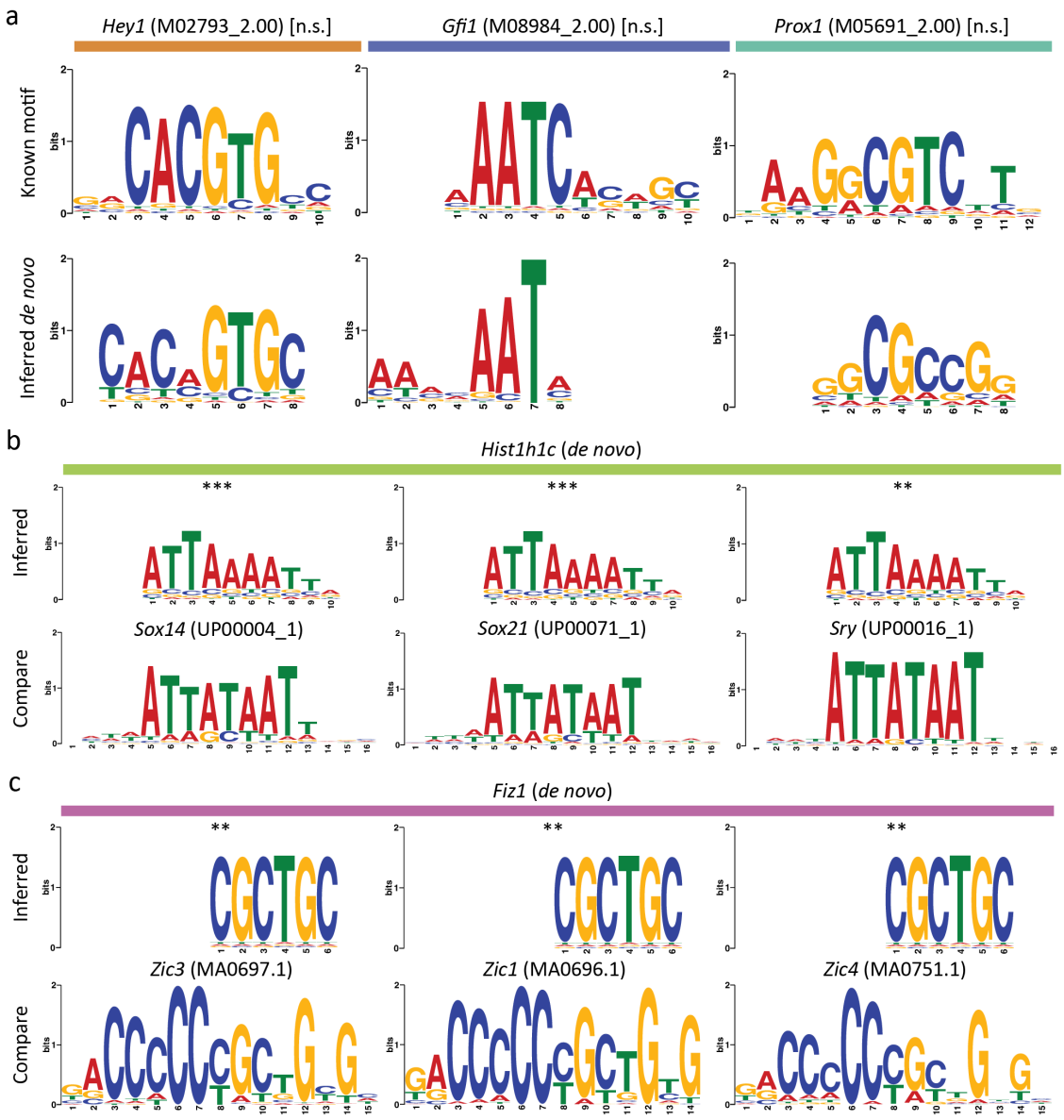

768

769 **Figure 5: Accurate target-gene predictions enable *de novo* discovery of DNA-binding motifs.**
770 **a.** Three examples of motifs enriched in the enhancer sequences of predicted target genes (bottom
771 row) which closely resemble known DNA-binding motifs (top row) for transcription factors with
772 at least one predicted target gene in the transcription factor-only hair cell gene-regulatory network.
773 **b, c.** Sequences for cofactors or putative transcription factors may represent novel DNA-binding
774 motifs or indicate sequence-specific interactions through multi-protein complexes. Motifs for two
775 hair cell genes closely match known DNA-binding sequences, suggesting that the linker histone
776 Hist1h1c (**b**, top row) forms complexes with SoxB2/A factors (**b**, bottom row), and that the

777 putative C2H2 zinc-finger protein Fiz1 (**c**, top row) recognizes motifs similar to Zic-family C2H2
778 zinc-finger proteins (**c**, bottom row). The statistical significance of each motif alignment was
779 estimated using the cumulative density function of all possible comparisons of known motifs
780 across enriched sequences for **a,** or inferred motifs across all database motifs for **b** and **c** (**,
781 $P \leq 0.01$**; ***, $P \leq 0.001$).
782

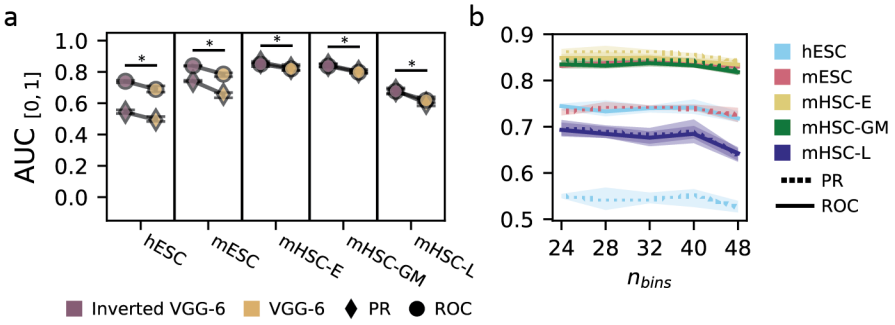

783

784 **Supplementary Figure 1: The inverted VGG-6 network outperforms a conventional VGG-6.**
785 **a.** Utilizing a more expressive feature space at the top of the network allows the inverted VGG-6
786 to outperform a conventional VGG-6 network when trained on the same input data. **b.** Performance
787 of the inverted VGG-6 network is robust across input-matrix sizes. Error bars and markers in **a**
788 and **b** show the full range and average performance across five cross-validated models. The
789 statistical significance in **a** was assessed using a one-sided Wilcoxon signed-rank test (*, $P \leq 0.05$).
790

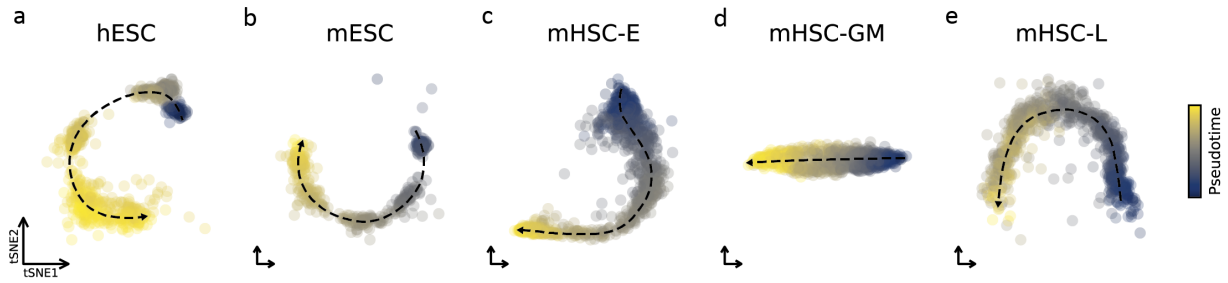

Supplementary Figure 2: Inferred pseudotime trajectories for the five training datasets. Two-dimensional embeddings of the trajectories for human embryonic stem cells (**a**), mouse embryonic stem cells (**b**), and mouse hematopoietic stem cells (**c-e**) were generated from the differentially expressed genes identified in BEELINE and colored by the inferred Slingshot pseudotime values.

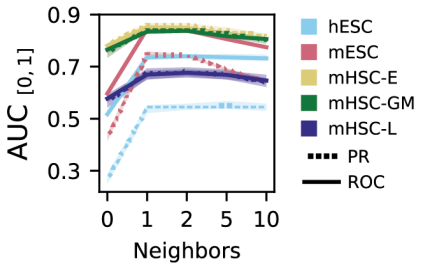

Supplementary Figure 3: Neighbor-gene matrices improve the neural network's performance.

Training the network on joint-probability matrices of up to two highly correlated neighbor genes increases performance across all datasets. Error bars and lines show the full range and average performance across five cross-validated models.

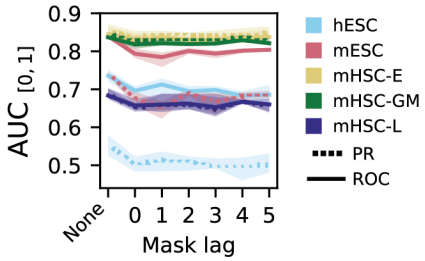

Supplementary Figure 4: Augmenting input matrices decreases the network's performance. Even though performance increases the most when training DELAY on input matrices from up to a single pseudotime lag, testing on channel-masked inputs suggests that the network relies on all available inputs, even gene-coexpression matrices from pseudotime lags two through five. Error bars and lines show the full range and average performance across five cross-validated models.

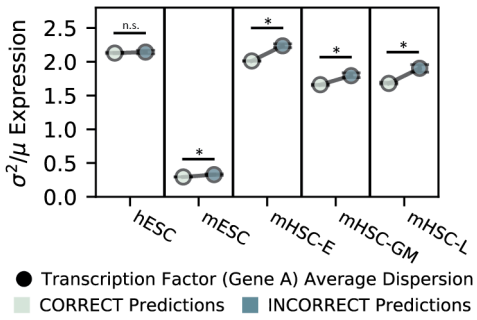

Supplementary Figure 5: DELAY performs best on transcription factors with stable gene expression.

An analysis of statistical dispersion across transcription factors shows that on average correctly inferred examples have lower variance-to-mean ratios than those of incorrect predictions. Error bars and markers show the full range and mean values across predictions from five cross-validated models. The statistical significance was assessed using a one-sided Wilcoxon signed-rank test (*, $P \leq 0.05$).

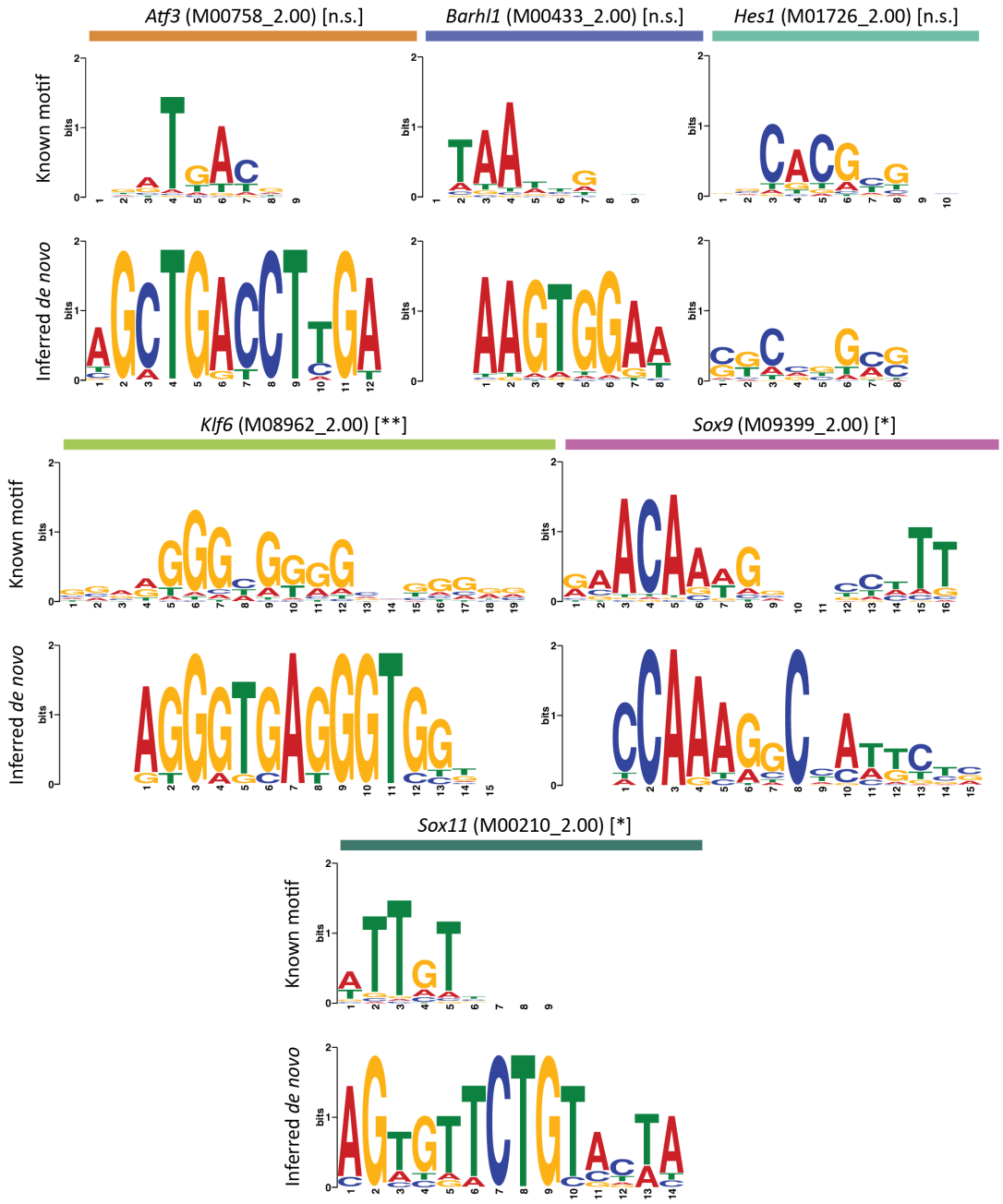

Supplementary Figure 6: Discriminative motif analysis corroborates gene-regulatory predictions.

Six additional examples of enriched motifs in the enhancer sequences of predicted target genes which closely resemble known DNA-binding motifs for transcription factors with at least one predicted target gene in the transcription factor-only hair cell gene-regulatory network. The statistical significance of each motif alignment was estimated using the cumulative density

828 function of all possible comparisons of known motifs across enriched sequences (*, $P \leq 0.05$; **,

829 $P \leq 0.01$).

830

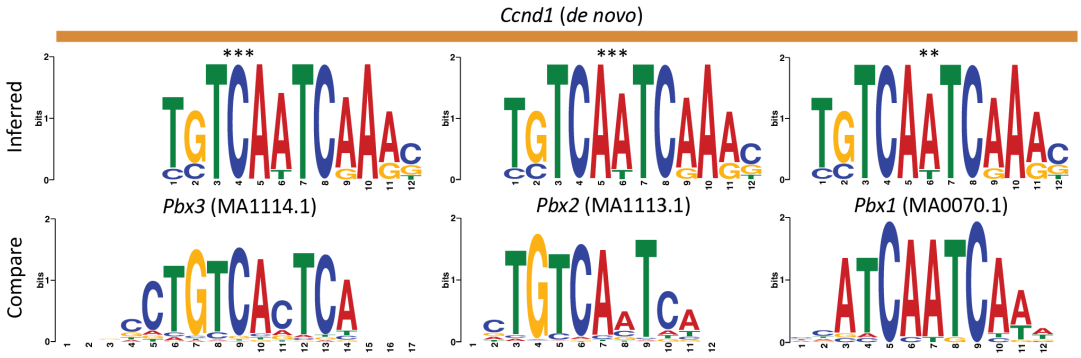

Supplementary Figure 7: An enriched motif in the enhancers of Ccnd1's predicted target genes suggests a mechanism for cofactor-target interactions.

An enriched motif in the enhancer sequences of cyclin Ccnd1's predicted target genes (top row) suggests that the putative cofactor forms complexes with Pbx-family homeobox transcription factors (bottom row) to regulate its target genes in a sequence-specific manner. The statistical significance of each motif alignment was estimated using the cumulative density function of all possible comparisons of the inferred motif across all database motifs (**, $P \leq 0.01$; ***, $P \leq 0.001$).